ChemPubSoc Europe

DOI: 10.1002/open.201800101

Open Access ChemistryOPEN Full Papers

Successful Synthesis of Gold Nanoparticles through Ultrasonic Spray Pyrolysis from a Gold(III) Nitrate Precursor and Their Interaction with a High Electron Beam

Mohammed Shariq,[a, b] Bernd Friedrich,[c] Bojan Budic,[d] Nejc Hodnik,[d] Francisco Ruiz-Zepeda,[d] Peter Majerič,[a, e] and Rebeka Rudolf*[a, e]

Herein, we report for the first time the successful preparation of a gold(III) nitrate [$Au(NO_3)_3$] water-based precursor for use in a bottom-up ultrasonic spray pyrolysis (USP) process. Due to its limited solubility in water, the precursor was prepared under reflux conditions with nitric acid (HNO_3) as the solvent and ammonium hydroxide (NH_4OH) as a neutralizer. This precursor enabled the USP synthesis of gold nanoparticles (AuNPs) and the in situ formation of low concentrations of NO_2^- and NO_3^- ions, which were caught directly in deionized water in a collection system. These ions were proven to act as stabilizers for the AuNPs. Investigations showed that the AuNPs were monodispersed and spherically shaped with a size distribution over three groups: the first contained 5.3% AuNPs with diameters ($2r$) <15 nm, the second contained 82.5% AuNPs with $2r$ between 15 and 200 nm, and the third contained 12.2% AuNPs with $2r>200$ nm. UV/Vis spectroscopy revealed the maximum absorbance band of the AuNPs at $\lambda=528$ nm. Additionally, scanning transmission electron microscopy (STEM) observations of the smallest AuNPs ($2r<5$ nm) revealed atomically resolved coalescence phenomena induced by interaction with the electron beam. Four stages of the particle-growth process were distinguished: 1) movement and rotation of the AuNPs; 2) necking mechanism; 3) orientated attachment at matching facets; 4) reshaping of the AuNPs by surface diffusion. This provided important insight into the formation/synthesis process of the AuNPs.

1. Introduction

Gold nanoparticles (AuNPs) have emerged as an excellent material for applications in chemical and biological sensing,[1] renewable energy (solar cells[2,3]), catalysis,[4,5] and biomedical applications[6–13] (drug delivery, imaging, and therapeutic agents) due to their specific unique properties such as surface plasmon resonance (SPR) and high biocompatibility.[14] SPR causes the oscillation of conduction electrons on the surface of the nanoparticles, stimulated by incident light, and thus, AuNPs have good physical, chemical, and optical properties.[15,16] As gold (Au) is known as the most corrosive-resistant metal in this world,[17] AuNPs also have the same nature. Moreover, AuNPs are biologically unreactive and, due to their high surface area to volume ratio, they can be conjugated and functionalized with proteins, peptides, and medical drugs.[18,19]

During the last two decades, much effort has been devoted to the development of production/synthesis techniques, and the different approaches focus on control of the parameters to reach an appropriate size, morphology, stability, or functionality of the AuNPs. The different production methods can be divided into bottom-up and top-down approaches. Bottom-up approaches include sol–gel, chemical vapor deposition, flame spray synthesis, various pyrolysis, and atomic or molecular condensation.[20–22] Top-down approaches include laser ablation, nanolithography, and high-energy milling.[23,24] Currently, these methods are suitable for the production of small quantities of nanoparticles (NPs) with major variations in the shapes and sizes of the NPs as a result of the production of different batches. The emerging technique of choice for the mass production of AuNPs is ultrasonic spray pyrolysis (USP).[25,26] It belongs to the pyrolysis class and is a synthesis technique that is capable of producing continuous metal and metal-oxide NPs with different sizes and morphologies. It has numerous advantages over conventional wet-chemical methods, as it is rela-

[a] M. Shariq, Dr. P. Majerič, Prof. R. Rudolf
University of Maribor
Faculty of Mechanical Engineering
2000 Maribor (Slovenia)
E-mail: rebeka.rudolf@um.si

[b] M. Shariq
Department of Mechanical Engineering
Indian Institute of Technology (Indian School of Mines) Dhanbad
826004 Jharkhand (India)

[c] Prof. B. Friedrich
IME Institute, RWTH Aachen
52056 Aachen (Germany)

[d] Dr. B. Budic, Dr. N. Hodnik, Dr. F. Ruiz-Zepeda
National Institute of Chemistry
1000 Ljubljana (Slovenia)

[e] Dr. P. Majerič, Prof. R. Rudolf
Zlatarna Celje d.o.o
3000 Celje (Slovenia)

Supporting Information and the ORCID identification number(s) for the author(s) of this article can be found under: https://doi.org/10.1002/open.201800101.

tively simple in construction, flexible in that different ranges of materials with narrow size distributions and varied shapes can be synthesized, and even economical, as it operates continuously at ambient pressure and temperature.[27–29] USP comprises the following stages: 1) formation of micron-sized aerosol droplets of the starting water solution of the metal salt by atomization through ultrasonic nebulizers and their transport through the carrier gas nitrogen (N_2); 2) evaporation of the solvent content of the aerosol droplets of the metal salt; 3) chemical reduction and thermal decomposition of the dried solute particles of the metal into NPs with the help of a reducing agent [such as hydrogen (H_2)]; 4) collection of the synthesized NPs in the desired suitable form (colloidal suspension or dry powder). There are a number of mechanisms associated with the transformation of aerosol droplets into the final NPs, but the most studied are droplet-to-particle and gas-to-particle mechanisms. Therefore, it is understandable that the size distribution of the formed NPs is mostly defined by the aerosol droplet size distribution. The correlation formulated by Lang[30] can be used to calculate these droplet sizes (see details in the Supporting Information, Section S A). The evaporation and reaction stages depend on the residence time of the aerosol precursor droplets at the evaporation zone and the dried solute particles at the reaction zone. The residence time of the droplets/particles inside the reaction zones is influenced mostly by the kinematics of the gas flow rate. It is important that the particle formation time must be shorter than the residence time of these aerosol droplets so that they can be transformed into the final AuNPs.[31] Calculation of the residence time can be found in Section S B.

In the synthesis of AuNPs, tetrachloroaurate in hydrate form [$HAuCl_4 \times H_2O$, so-called gold(III) chloride] is the most commonly reported and used precursor mainly due to its complete solubility in common solvents such as water.[32–36] However, this precursor causes the in-growth and transformation of AuNPs into a polydisperse size-range distribution and also poisons the active surfaces of the AuNPs. Polydispersity in the size distributions of the AuNPs is a result of the formation of large clusters due to coalescence and agglomeration phenomena, whereas poisoning of the active sites limits the functionality of AuNPs in different biomedical and catalysis applications.[37–41] Although many attempts with different stabilizers, such as sodium citrate and polyethylene glycol, in the past years have been made to control and eliminate these effects from the use of an $HAuCl_4$ precursor, they have all been unsuccessful. Apart from this, other chloride-free precursors, such as $Au(NO_3)_3$, gold(III) acetate [$Au(CH_3COO)_3$], gold(I) bromide (AuBr), and gold(III) hydroxide [$Au(OH)_3$], have been proposed as promising candidates.[42–45] These gold salts were reported to be solid and crystalline at low relative humidity (RH), partially insoluble in common solvents, and, in addition, usually decompose in water.[46–48] In the literature, $Au(CH_3COO)_3$ was shown to have tremendous potential to expand the composition and architecture of AuNPs.[49] In the last reported work, our research group showed and investigated the successful preparation of the precursor of AuNPs starting from $Au(CH_3COO)_3$ in addition to the synthesis of AuNPs in water solutions by using USP. This resulted in the presence of a small amount of Cl^- ions in the colloidal suspension of the AuNPs. Thereby, the search for a chloride-free precursor has continued and has opened the path for $Au(NO_3)_3$ as the next promising candidate. In a U.S. patent,[42] the $Au(NO_3)_3$ precursor was prepared by dissolving gold(III) oxide powder in concentrated HNO_3. However, the literature lacks content in the direct use of commercially available $Au(NO_3)_3$ powder, which is poorly soluble in water. Therefore, investigation of the whole process of preparing a soluble and chemically stable water-based $Au(NO_3)_3$ precursor is highly important and remains a major challenge for further use in the synthesis of AuNPs.[51] Thus, it deserves deep exploration.

In the best of the reported works to date, the chemical preparation of the commercially available $Au(NO_3)_3$ precursor was not previously studied with USP. Consequently, the main aim of this work was to test and establish $Au(NO_3)_3$ as a new and reliable Cl^--free precursor for the controlled scale-up USP synthesis of monodispersed colloidal AuNPs having spherical shapes and final higher concentrations in suspension form. On this basis, the preparation of $Au(NO_3)_3$ herein presented does not suffer from any chemical solubility or stability issues, and the process can be scaled up for the USP synthesis of AuNPs with different characterization techniques. The chemical reactivity of the $Au(NO_3)_3$ precursor was investigated through thermogravimetric analysis—differential thermal (TGA-DT) measurements, whereas the chemical properties of the synthesized AuNPs were determined through energy-dispersive X-ray (EDX) spectroscopy and optical emission spectrometry with inductively coupled plasma (ICP-OES) analysis. The physical properties of the AuNPs were interpreted with the help of transmission electron microscopy (TEM), dynamic light scattering (DLS), and ultraviolet-visible (UV/Vis) spectroscopy measurements. The electron interaction phenomena of the AuNPs were investigated with the use of the scanning transmission electron microscopy (STEM) technique.

2. Results and Discussion

The investigation and testing of $Au(NO_3)_3$ as a new precursor for the synthesis of AuNPs through USP depends on its chemical reactivity in the high- and low-temperature ranges and its chemical solubility in water-based solution. The reactivity was investigated through TGA-DT measurements, and its solubility was tested through mechanical (magnetic stirring with heating and ultrasonication) and chemical decomposition methods (heating under reflux conditions). After the successful preparation of the stable $Au(NO_3)_3$ precursor, it was inspected for several trials in USP before the optimal parameters for evaporation, reaction-zone temperatures, and gas flow rates of the carrier and reducing gases were found.

2.1. Thermal Analysis of the Decomposition of $Au(NO_3)_3$

In understanding the process of preparing the new $Au(NO_3)_3$ precursor for the synthesis of AuNPs through USP, TGA-DT analysis helped in determining the chemical decomposition reactions of $Au(NO_3)_3$, in addition to its decomposition tempera-

tures and the intermediate byproducts formed, if any. The analysis depended strongly on the kinematic parameters (heating rate, carrier gas, and flow rates) and thermodynamic parameters (decomposition temperature ranges). Complete thermal decomposition of metal nitrates [e.g. $Au(NO_3)_3$] usually occurs in two stages: chemical dissociation and reduction. In general, decomposition is initiated by dissociation of the N–O bond present in the nitrate ion. As $Au(NO_3)_3$ is heated, sublimation takes its initial course, which gives stable molecular vapors, and this is followed by decomposition into metal cations (Au^{3+}) and nitrate anions (NO_3^-). The metal cation influences the decomposition reaction through its ability to distort the nitrate ion.[52–54] Finally, reduction of the Au^{3+} cation into pure Au at a high temperature takes place.

The TGA-DT curves obtained during heating of $Au(NO_3)_3$ show complete dissociation over two endothermic stages within different temperature ranges (Figure S1: TGA-DT). The first step can be attributed to initial decomposition, and it starts at about 80 °C and extends up to 160 °C with a weight-loss percent of 5.9%. This decomposition under a N_2 atmosphere does not have any noticeable influence on resultant anhydrous $Au(NO_3)_3$. As the dissociation of the N–O bond starts, the rate of decomposition of $Au(NO_3)_3$ will be fast, as the strength and bond order of the N–O bond decreases. On the other hand, Au^{3+} ions have a low charge density, which makes them ineffective in polarizing the NO_3^- ions at low decomposition temperatures. This behavior of the Au^{3+} ions will keep the NO_3^- ions intact together at lower temperatures until thermal forces overcome the ionic bond, which then leads to decomposition.[54] This overcoming of the thermal force occurs as a result of the second step, which occurs over the range of about 220 to 420 °C with a maximum weight loss of 16.9%. This results in complete dissociation of the Au^{3+} and NO_3^- ions. The final reduction of Au^{3+} into pure Au occurs in the range of 480 to 800 °C with 6.8% weight loss. Thus, to promote the evaporation of the aerosol droplets and thermal decomposition for chemical conversion and nucleation and growth of the AuNPs from $Au(NO_3)_3$ in the USP, the evaporation temperature should be kept in the range of 140 to 160 °C, whereas the reaction temperature should be in the 500–600 °C range. The gas flow rates in both heating zones will lead to faster heating rates in USP. Thus, initial decomposition will start at a higher temperature than that measured by TGA-DT. As the residence time of the precursor in the reaction zone will be too short, a reduction gas, that is, H_2, is needed at the start of the reaction zone to obtain the AuNPs. Some experimental trials were done in the absence of H_2 gas, and no AuNPs were formed.

The decomposition reaction can be predicted as [Eqs. (1) and (2)]:

$$Au(NO_3)_3 \rightarrow Au^{3+} + NO_3^- + NO_2^- \quad (1)$$

$$Au^{3+} + NO_3^- + NO_2^- \rightarrow Au + NO_3^- + NO_2^- \quad (2)$$

2.2. Preparation of the $Au(NO_3)_3$ Precursor and Synthesis of AuNPs

$Au(NO_3)_3$ was tested to increase its solubility in water; however, the desired clear yellow solution was obtained only with heating under reflux conditions ($T \leq 100$ °C, $t = 1$ h; Figures 1b and S1: USP). HNO_3 with a 35% water content was added as the solvent. The $Au(NO_3)_3$ solute powder did not take up the added solvent significantly until a critical RH limit and solubility were reached. After 45 min, a phase transition occurred, and the solute particles were dissolved, which produced a saturated solution that was used with USP. As this solution was highly acidic (pH 0–1) and could damage the membranes of the ultrasonic generator if used, NH_4OH with a 75% water content was added for neutralization (pH 6–7). This unique combination, containing Au^{3+}, NO_3^-, and NH_4^+ ions and an H_2O molecule, is shown in Figure 1d as the precursor. This solution was found to be stable for about 1 month. Consequently, due to the NO_3^- and NH_4^+ ions, NH_4NO_3 was formed as a byproduct in the reaction. The addition of HNO_3 and NH_4OH slightly changed the rheological properties relative to those of deionized water (see Table 1). The density of the combination solution was higher than that of deionized water, and thereby, the USP generator required a bit more input power to produce the same amount of aerosol as that produced with other water-based precursors. The lower value of the surface tension allowed more stable aerosol droplets to be formed, which consequently resulted in spherically shaped AuNPs.[55]

The precursor contained more than half its volume in water molecules because of the initial dilution, and a thick cloud of aerosol, called the primary droplets, was formed in the generator as desired (Figure 1d: aerosol droplet). The droplets were carried into the evaporation zone, maintained at $T \leq 150$ °C, with the help of N_2 as the carrier gas, and in this zone they began to evaporate and shrink. This shrinkage and dehydration of the water content from the solute particles of $Au(NO_3)_3$ increases the concentration of Au inside the evaporated droplet[56,57] (Figure 1d: evaporation).

Microexplosions of these primary droplets then occurred to give smaller droplets, and this led to the formation of secondary droplets in the reaction zone maintained at $T \leq 600$ °C. This occurred due to supersaturation and precipitation phenomena of the concentrated solute. These dried precipitated particles then underwent thermal conversion and fast reduction with the help of H_2 gas to give fine AuNPs.[58,59] The role of H_2 gas as a reducing agent in the reaction zone was to provide sufficient reduction energy for the dried aerosol particles containing Au^{3+} ions to be converted into pure AuNPs. By using H_2 gas in the reaction zone, the required temperature for the creation of AuNPs could be reduced considerably relative to the neutral atmosphere.[57] The intermediate product, ammonium nitrate (NH_4NO_3), in the aerosol droplets after the evaporation of water started to melt and immediately decomposed due to the high temperature of the reaction zone (≈ 600 °C). NH_4NO_3 decomposes to N_2O and water at temperatures of 170–400 °C, whereas at temperatures above 400 °C, it may decompose into water, nitrogen, and NO or into water, ni-

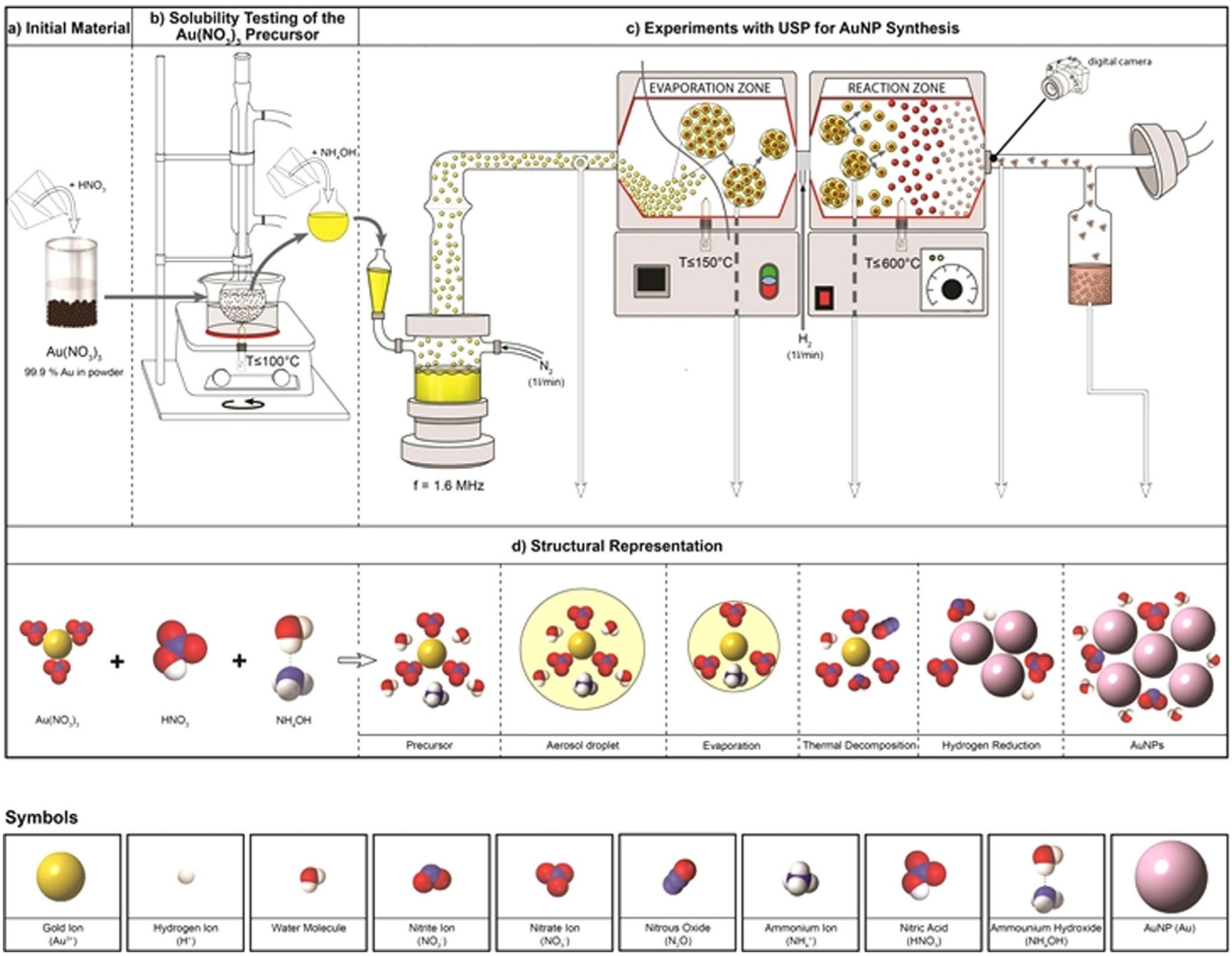

Figure 1. Schematic representation of the synthesis of AuNPs from the $Au(NO_3)_3$ precursor. a) initial material and b) solubility testing of the $Au(NO_3)_3$ precursor: HNO_3 was added to the initial $Au(NO_3)_3$ powder. The mixture was heated at reflux at $T \leq 100\,^{\circ}C$ and a yellow-colored solution was obtained with pH 0–1. NH_4OH was added to neutralize the refluxing solution to pH 6–7. A solution of the $Au(NO_3)_3$ precursor was achieved with a gold concentration of 2.5 g L^{-1}. c) Experiments with USP for AuNPs synthesis: an ultrasonic generator with a frequency of 1.6 MHz created aerosol droplets from the precursor, and these droplets were carried away in quartz transport tubes with the help of N_2 as the carrier gas (1 L min^{-1}) to the evaporation zone (maintained at 150 °C) and reaction zone (maintained at 600 °C). H_2 gas (1 L min^{-1}) entered directly the reaction zone and was used as a reducing agent. The AuNPs were collected in deionized water in bottles (seen as a pink-colored solution). A digital camera located at the end of the reaction zone was used to measure the area covered by aerosol droplets in the evaporation zone. d) Structural representation: it represents schematically the initial ionic state, as well as their changes from the precursor solution to AuNPs at different stages: precursor preparation, aerosol droplet generation, evaporation of water and shrinkage of aerosol droplet, thermal decomposition, hydrogen reduction, and collection of AuNPs in deionized water with NO_3^- and NO_2^- ions.

Table 1. Rheological properties of the prepared $Au(NO_3)_3$ precursor, HNO_3, and NH_4OH compared with those of deionized water (measured at 21 °C).

Precursor solution component	Density [g cm^{-3}]	Viscosity [MPa s]	Surface tension [mN m^{-1}]
$Au(NO_3)_3 + HNO_3 + NH_4OH$	1.2 ± 0.3	2.1 ± 0.1	41.6 ± 0.2
deionized H_2O	1.0 ± 0.1	1.0 ± 0.2	72.7 ± 0.2

trogen, and NO_2.[60,61] Upon heating NH_4NO_3 quickly, products such as water, nitrogen, and oxygen or water, nitrogen, NO, and NO_2 are most likely to be formed.[62] With the help of ion-chromatography detection tests, it was confirmed that NO_2^- and NO_3^- ions were formed (Figure 1 d: thermal decomposition and hydrogen reduction). The final AuNPs were collected in bottles containing deionized water. The NO_2^- and NO_3^- ions were also subsequently carried away to collection bottles (Figure 1 d: AuNPs). The in situ formation of these ions played an important role in the stabilization of the AuNPs in deionized water and over the course of 9 months prevented agglomeration and coagulation of the AuNPs. Thus, no additional stabilizer was required in the final collection state.

The gas flow rates of H_2 and N_2 were found to affect the kinematics of the mechanism of formation of the AuNPs in the reaction chamber. It was determined that at high flow rates of the N_2 and H_2 gases (each 2 L min^{-1}), the residence times of the aerosols and dried particles calculated at the evaporation

and reaction zones were 1.8 and 0.6 s, respectively. This total retention time of 2.4 s was not sufficient for complete conversion of $Au(NO_3)_3$ into the AuNPs. This resulted in the transparent color of the final collected solution of water due to incomplete thermal conversion. At medium flow rates of 1.5 L min^{-1}, the residence times were 2.4 and 0.7 s, respectively, with a total of 3.1 s. This flow was also not sufficient to complete the formation mechanism. Therefore, the flow rate was reduced further to 1 L min^{-1} and, as a consequence, the residence time increased to 3.7 and 0.8 s (total of 4.5 s). These parameters were sufficient for successful results. A schematic illustration of the complete mechanism is shown in Figure S2. Calculation of residence times can be found in Section S B. The cross-sectional areas covered by the aerosol at these gas flow rates in the transport tubes were measured at the entering surface plane in the evaporation zone with the help of a digital camera (Figure S2). The calculated percentages of cross-sectional areas covered at high, medium, and low gas flow rates were 52.0, 45.9, and 38.4% of the entering plane, respectively. Upon going from high to low gas flows, the volume of the aerosol entering the evaporation zone decreases. The lowest volume was the most optimum to complete the process.

2.3. Size Distribution through DLS and ζ Potential

The principle of DLS is based on Rayleigh scattering, which occurs due to the Brownian motion of AuNPs that are smaller in size than the incident light wavelength at a fixed scattering angle.[63] The reason behind choosing this technique for the size distribution is due to the spherical shape of the NPs, which was already assumed in the analysis. DLS analysis revealed three different groups of particles with different size distributions (in number percent): group 1 contained 5.3% AuNPs with a diameter ($2r$) $<$ 15 nm, group 2 contained 82.5% AuNPs with $2r$ between 15 and 200 nm, and group 3 contained 12.2% AuNPs with $2r >$ 200 nm. A histogram of the DLS data is shown in Figure 2a. The surface ζ potential with standard deviation (SD) was (33.5 ± 2.1) mV. This value indicates the stability of the AuNPs and their ability to resist coalescence and agglomeration for up to a minimum of 9 months.[63]

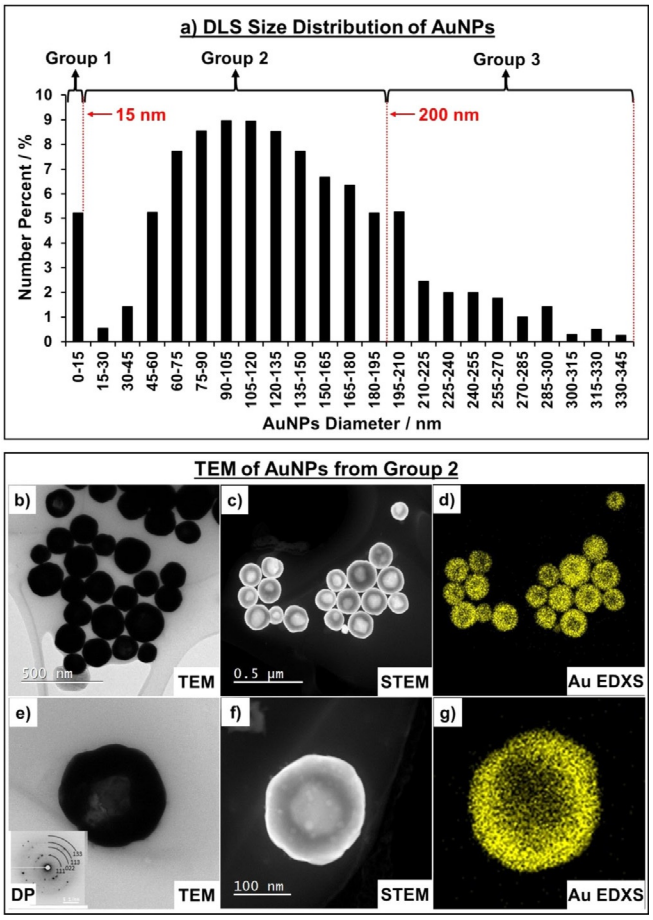

Figure 2. a) DLS size distribution of the AuNPs into three groups: group 1: 5.3% AuNPs in the size range of 0 to 15 nm, group 2: 82.5% AuNPs in the size range of 15 to 200 nm, and group 3: 12.2% AuNPs in the size range of above 200 nm. TEM characterization of AuNPs belonging to group 2: b) TEM bright field, c) STEM annular dark field (ADF) images of the synthesized AuNPs from $Au(NO_3)_3$, d) EDX spectroscopy Au elemental mapping of a group of AuNPs. e) TEM image of a single AuNP and its electron diffraction pattern displaying several spots matching the lattice distances of Au and indicating a polycrystalline nature. f) STEM ADF image of a single AuNP. g) EDX spectroscopy Au elemental mapping of the single AuNP showing a hollow center.

2.4. TEM Characterization

The AuNPs synthesized in the final confirmatory experiments were studied by TEM (Figures 2b,c). The particles exhibit a polycrystalline quasispherical shape with a hollow center (Figures 2e,f). It is possible to distinguish that the density of Au in a single AuNP is not uniform, probably due to the fact that the diffusion of [Au] during the sintering process is more prominent in the outer radius of the surface than in the center. This can be seen on the energy-dispersive X-ray (EDX) spectroscopy maps in Figure 2d,g, in which a lower Au signal is recorded at the center of the particles. The multiple spots from the electron diffraction pattern reveal that the AuNP is composed of several grains, and the measured distance corresponds well with the characteristic lattice distances of Au (Figure 2e). The AuNPs appear as a monodispersed suspension, as they do not agglomerate. The average mean diameter basically belongs to group 2 [(174.0 ± 35.8) nm]. These grouped size distributions are explained in the DLS measurement. The calculated circularity was 0.9 (within the 0–1 range; 0 signifies an irregular shape and 1 signifies a perfect circle).

In addition, by using STEM we observed the coalescence of uniformly dispersed 2–3 nm AuNPs under the influence of the raster electron beam probe (with a beam current of ≈14.5 pA at 80 kV). About 5.3% of the synthesized AuNPs are in the size range below 15 nm, and they are presumably leftover from the unfinished USP process (a small fraction of the sample, Figure 3a). The bigger particles (5–8 nm) are mostly round, but they also have defects such as twins. The overall examined area consists of AuNPs dispersed on the carbon film (Figures S3 and S4). If imaging at lower magnification in the STEM mode, the irradiation dose of the electron beam (e Å^{-2}) spreads out over a large region; additionally, if a fast scan rate is used

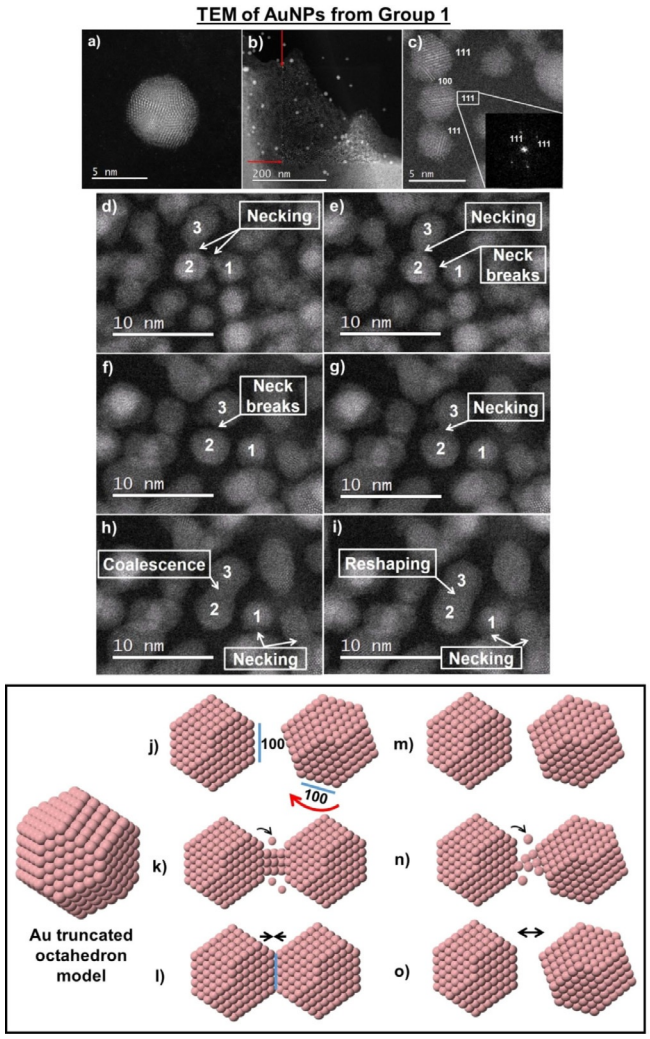

Figure 3. AuNPs (belonging to group 1) coalescence and reshape as a result of exposure to the electron beam, as observed by STEM. a, b) STEM ADF image of a small-sized AuNP and after beam exposure. c) AuNPs with crystal lattice planes indicated. d–i) STEM ADF images displaying the coalescence and reshaping of the AuNPs. It shows the sequence of the recorded images, each roughly after another demonstrating two particles that initiated necking but, however, did not merge into one. j–o) Atomic models of the coalescence of the AuNPs.

(typically 3–4 μs), the overall dose can be minimized due to the short time the beam spends on each spot. However, at higher magnification, that is, zooming into the region of interest to atomic resolution, the scanned area is reduced and the exposure time is increased, which increases the electron dose rate ($e Å^{-2} s^{-1}$). In our case, zooming in to an area of 27 nm^2 with a pixel size of 0.5 Å and a frame rate of 1.6 $s\,frame^{-1}$, the uniformly distributed AuNPs start to migrate, rotate, merge, and coalesce by ripening, necking, and reshaping, and this results in the formation of bigger AuNPs (Figures 3b, c).

The initial process occurs very fast and eventually reaches a steady state, at which apparently no more interaction is perceived for a long time. It was previously reported that damage from electron radiation influences the behavior of such NPs.[64–66] Depending on the type of bonding and the environment, radiolysis or knock-on causes the removal of the capping of the AuNPs and leaves a bare surface, which thus promotes contact between the neighboring AuNPs.[65] The drift experienced in our observations suggests that the intervening substance between the AuNPs is removed at the moment of observation. The observed process of AuNP growth can be divided into four stages: 1) AuNP movement and rotation; 2) necking mechanism; 3) orientated attachment at matching facets;[64] 4) subsequent reshaping or restructuring of the AuNPs by surface diffusion to lower the surface energy (Figures 3d–i). During this process, the AuNPs wiggle and/or reorient to meet similar facets from other nearby NPs.[65] At this point, "necking" takes place, which facilitates coalescence if the AuNPs are close. On the other hand, the diffusion of single atoms can also promote Ostwald ripening; however, as observed, in some cases no coalescence is observed at all, even if the NPs are very close and already showing signs of necking. Upon zooming out, two distinct regions are discerned (Figures 3b, S3E, and S3F): one area in which the AuNPs remain in a pristine shape (the region that was not exposed) and a second area in which bigger and elongated AuNPs are formed (the region in which the beam was rastered for a longer time). The proposed model of the occurring process is described in Figures 3j–o (see Video S1, demonstrating the whole phenomenon of coalescence and reshaping). After that, the formation of bigger, hollow AuNPs occurs. The exact mechanism of this process was not studied for the current paper and is the focus of our future studies, by which we will try to control the size and the ratio between the hollow core and the Au shell thickness. In the TEM image shown in Figure S7, one can see the early stage of hollow nanoparticle formation that already provides clues into the process (see additional Video S2).

2.5. UV/Vis Spectroscopy

UV/Vis spectroscopy is a reliable technique for determining the absorbance band and aggregation levels of the synthesized AuNPs. The maximum SPR bands appears at around $\lambda_{max} =$ 528 nm, which clearly suggests a stable state. The sharp and narrow band of the curve corresponds to its monodispersed nature without any aggregation (Figure S2: UV/Vis).

2.6. ICP-OES Analysis

The final concentration of the AuNPs collected in the final state was 210 ppm. Higher concentrations, with values of more than 1000 ppm, were achieved by rotary evaporator technology for further use in testing.

2.7. Ion Gas Chromatography

On the basis of ion-chromatography analysis, AuNPs in deionized water with a concentration of 210 $mg\,L^{-1}$ contain 5.8 mg of NO_3^- ions and 1.5 mg of NO_2^- ions, which is enough to stabilize the solution for more than 9 months, assuming the DLS size distribution of groups 1–3. By rough estimation, considering one layer of water covering the NPs and a diameter of 2.7 Å for a water molecule, it can be concluded that every par-

ticle in group 1 is covered by almost 5300 water molecules, and particles in groups 2 and 3 are covered by more than 381 500 molecules of water. However, Wang and Gunasekaran concluded that two shell-like structures of water molecules were formed around the surface of AuNPs.[21]

2.8. Yield Efficiency of the USP process

Upon using $Au(NO_3)_3$ as a precursor, the yield efficiency of the USP process was calculated to be 70% (Section S F), which is significantly higher than the yield efficiency obtained upon using $HAuCl_4$ as a precursor (<10%) under the same running conditions.[34] The higher value obtained in the former case can be attributed to the much lower deposition of AuNPs on the transport tubes, impaction, gravitational sedimentation in the transport tubes, diffusion onto the transport tube walls, turbulence, and thermophoresis.

3. Conclusions

We achieved in-depth understanding of the chemistry necessary to prepare a soluble and stable water-based $Au(NO_3)_3$ precursor by using HNO_3 and NH_4OH under reflux conditions. This enabled the synthesis of uniformly disperse aerosol droplets for the continuous ultrasonic spray pyrolysis (USP) synthesis of gold nanoparticles (AuNPs) and in situ formation of NO_3^- and NO_2^- ions, both of which were caught in deionized water. The ions played an important role in stabilizing the AuNPs for up to 9 months and precluded the use of any external surfactant. We also set up a model for the mechanism to convert the $Au(NO_3)_3$ precursor into final AuNPs at optimal temperatures for the evaporation and reaction zones and optimal gas flow rates of the carrier and reducing agents. It was demonstrated successfully that with lower flow rates of the carrier (H_2) and reducing (N_2) gases, these aerosol droplets had sufficient residence times to be completely converted into the AuNPs from $Au(NO_3)_3$. The observed phenomena were resolved atomically by transmission electron microscopy, by which small-sized AuNPs ($2r < 15$ nm) exhibited dynamic coalescence under the influence of the electron beam. The transfer of Au atoms from one AuNP to another with the combined phenomena of necking, breaking, coalescence, and reshaping were proposed as the mechanisms for particle growth. Our observations provide important insight into the formation/synthesis process of AuNPs. These AuNPs will be tested further for different applications.

Experimental Section

Materials

$Au(NO_3)_3$ (American Elements, USA, 99.9%), HNO_3 (65%, Honeywell Fluka GmbH, Germany), NH_4OH solution (≈25% NH_3 basis, Honeywell Fluka GmbH, Germany), deionized water (purified with the Millipore system), N_2 (99.9%, Westfalen AG, Germany), and H_2 (99.9%, Westfalen AG, Germany).

TGA-DT Measurement

Equipment: PerkinElmer TGA-4000. Initial parameters (set standardly): mass of $Au(NO_3)_3$ sample: 10.5 mg, inert gas: N_2, gas flow rate: 20 mL min^{-1}, heating rate: 50 °C min^{-1}, temperature range: 50–900 °C. The sample was heated in a standard platinum crucible; temperature accuracy: ±1 °C, temperature precision: ±0.8 °C.

Detailed Description of the Procedure to Increase the Solubility of $Au(NO_3)_3$

Magnetic Stirring with Heating

The received $Au(NO_3)_3$ powder was dark brown containing micron-sized particles (Figure 1a). Initially, $Au(NO_3)_3$ (0.1 g) was added to HNO_3 (30 mL) to have a Au concentration of 1 g L^{-1}. The mixture was stirred for about 1 h with subsequent heating up to 60 °C. As the temperature reached about 35 °C, particles began to decompose. At 45 °C, insoluble particles continued to decompose, turning the solution dark brown. At about 55 °C, the degree of decomposition increased; however, a large number of particles started to settle down at the bottom as sedimentation. Finally, some particles remained insoluble (Figure S1).

Ultrasonication

Initially, ultrasonication was started with $Au(NO_3)_3$ (0.04 g) mixed with HNO_3 (20 mL) to have a Au concentration of 1 g L^{-1}. The factors were 35% for the amplitude of the ultrasound, and 0.3 per second for the cycle of application (in percent terms, an ultrasound application cycle of 0.3 per second was equivalent to 30%). The insoluble solution stayed dense and dark brown and remained in the same state till the temperature reached 60 °C (Figure S1).

Reflux Boiling of $Au(NO_3)_3$ with Nitric Acid

$Au(NO_3)_3$ (0.02 g) was added to HNO_3 (10 mL) to have a Au concentration of 1 g L^{-1}, and the mixture was heated continuously under reflux conditions. After 30 min, the solution appeared to be clear and yellowish in color and completely solubilized. The pH value was in the range of 0 to 1. This high acid content is not recommended to be used in ultrasonic generators, as it can potentially damage the thin coating of the quartz glass coating on the surface of the nebulizer membranes in the USP instrument. Therefore, the solution was neutralized by adding NH_4OH (13 mL) to achieve a pH value of 7 (Figures 1b and S1).

The neutralized precursor was kept in small glass bottles at room temperature for about 1 month to test its stability. It was noticed that the white-colored NH_4NO_3 salt was formed at the cap opening of the bottle due to its interaction with the atmosphere. This salt formation could cause blockage of the transport tubes in the reaction zones during the synthesis of the AuNPs. Therefore, further investigation of the decomposition behavior at different heating rates and confirmation of complete removal of this salt through TGA-DT was needed (Figure S5). Thus, it could be concluded from the analysis that the decomposition of NH_4NO_3 at a low heating rate of 10 °C min^{-1} (this rate was chosen to obtain all the chemical decomposition data) and a high heating rate of 50 °C min^{-1} (to simulate the conditions of USP during the synthesis process) occurred in the temperature range of 150 to 350 °C. The reaction zone temperatures during the synthesis of the AuNPs from $Au(NO_3)_3$ were higher than 350 °C, so that the intermediate NH_4NO_3 byproduct

was completely decomposed in the transport tubes in the USP instrument.

Continuing with the trials for higher Au concentrations under reflux conditions, $Au(NO_3)_3$ (0.01 g) was added to HNO_3 (1 mL) to have a Au concentration of 5 g L^{-1}. NH_4OH (up to ≈1.3 mL) was added into the refluxing yellow solution to raise the pH up to 6–7. The solution was diluted further by adding deionized water (1 mL). The solution suddenly became unstable and a brown precipitate formed, which proved that this method was also inappropriate for use with USP. A possible cause for the formation of the precipitate could be the increased concentration of HO^- ions due to the water and NH_4OH, which caused instability of the precursor. To make the solution stable and to reduce the presence of HO^- ions, only NH_4OH could be added for the purpose of neutralization and dilution.

Final Trial

This final trial was performed to test the chemical stability of $Au(NO_3)_3$ with HNO_3 at higher Au concentrations with NH_4OH only. Therefore, $Au(NO_3)_3$ (0.01 g) and HNO_3 (1 mL) to have a Au concentration of 5 g L^{-1} were mixed continuously under reflux. NH_4OH (up to 1.3 mL) was added, and the pH was raised to a value of 7. The refluxing solution was diluted further with NH_4OH to lower the concentrations and it remained stable.

Final Preparation of the Precursor Solution

$Au(NO_3)_3$ (3 g) was added to HNO_3 (300 mL), and the mixture was heated under reflux conditions. Small aliquots (20 mL) of NH_4OH (to a total of 300 mL) were added with continuous stirring and cooling of the yellow precursor. The solution was neutralized successfully and diluted to a final Au concentration of 2.5 g L^{-1}.

Measurement of the Density, Viscosity, and Surface Tension of the $Au(NO_3)_3$ Precursor Solution

Density

Approximated as a weighted average of constituents on a volume basis. The average calculated density was found to be (1.2 ± 0.3) g cm^{-3}.

Viscosity

A Fungilab Smart Series Rheometer with a low viscosity adapter (LCP/B) (Barcelona, Spain) was used to determine the viscosity of the $Au(NO_3)_3$ precursor. The average calculated value was (2.1 ± 0.1) MPa s.

Surface Tension

Determined with the Wilhelmy plate method with a KRŰSS K12 tensiometer. A platinum plate was suspended vertically and immersed into the liquid. The surface tension was calculated from the contact angle and the force, which correlates with the surface tension and the length of wetting. Measurements were repeated three times for every sample, and in one repeat, ten measurements were made. The calculated value was (41.6 ± 0.2) mN m^{-1}.

USP Process Equipment

The trial, as well as the final run, for the synthesis of AuNPs were performed on a redesigned modular USP located at the IME Institute of Process Metallurgy and Metal Recycling, RWTH Aachen, Germany (Figures 1c and S1: USP). It comprised the following main parts: ultrasonic generator, evaporation zone, reaction zone, collection bottles, and transport tubes. It was redesigned for separating the heating zones into two, maintained at T_1 and T_2 respectively. An ultrasonic aerosol generator (Gapusol, RBI France with piezoelectric transducer membrane, having a frequency of 1.6 MHz and intensity 0–9) was used to generate aerosol droplets of the precursor. These aerosol droplets were then transported through a quartz tube (length = 28 cm and diameter = 2 cm) to the heating zones of the equipment. Dry N_2 was used as the carrier gas, and H_2 was used for reduction into the final AuNPs. The collection bottles contained deionized water as a solvent. Transport of the aerosol into the evaporation zone was recorded with a digital camera (NIKON COOLPIX P500) placed at the end point of the reaction zone.

Synthesis of AuNPs with USP

USP Trial 1

The final $Au(NO_3)_3$ precursor was used with the following parameters, as mentioned in Table 2. The collection bottles were transparent, thereby implying no formation of AuNPs (Figure S1). Possible reasons could be a low reaction temperature (400 °C) and low residence time (i.e. 2.4 s).

USP Trial 2

The reaction temperature was increased to 500 °C (Figure S1) and the gas flow rates were decreased to 1.5 L min^{-1} to achieve longer residence times (3.1 s). Still, the collection bottles were transparent, implying no formation of AuNPs.

Table 2. Parameters considered in USP.[a]

USP trial	[Au] [g L^{-1}]	T_1 [°C]	T_2 [°C]	Flow rate [L min^{-1}] N_2	H_2	t_{exp} [h]	Solvent	t_R [s] Evaporation zone	Reaction zone	t_{tot} [s]
1	2.5	150	400	2.0	2.0	4	deionized water	1.8	0.6	2.4
2	2.5	150	500	1.5	1.5	4	deionized water	2.4	0.7	3.1
3	2.5	150	600	1.0	1.0	4	deionized water	3.7	0.8	4.5

[a] [Au]: concentration of Au in the $Au(NO_3)_3$ precursor, T_1: evaporation zone temperature, T_2: reaction zone temperature, t_{exp}: duration of the experiment, t_R: residence time in the evaporation or reaction zone, and t_{tot}: total residence time; initial frequency of the nebulizer = 1.6 MHz, ambient temperature = 21 °C.

USP Trial 3

The reaction temperature was increased further to 600 °C (Figure S1), whereas the flow was decreased to 1 L min^{-1}. The collection bottles showed a pink-colored solution, indicating the formation of AuNPs.

Final Set of Experiments

The final experiments were performed with the same parameters as those determined by USP trial 3. Theoretical measurement of the aerosol droplets of the precursor was calculated to be 2.3 μm.

Characterization Techniques of AuNPs

DLS and ζ Potential Measurements

The size distribution and ζ potential of the AuNPs were investigated at 25 °C by means of DLS by using a Malvern Zetasizer Nano ZS scattering apparatus (Malvern Zetasizer Nanoseries Instruments Ltd., Worcestershire, U.K) and a colloidal suspension of the AuNPs. The size distribution was measured with disposable plastic cuvettes, and the ζ potential was measured by a dip cell provided with electrodes. The initial parameters for the measurements were: refractive index = 0.2, absorptivity = 3.3; dispersant properties: water temperature = 25 °C, equilibration time: 25 s, measurement angle: 173° backscatter; particle-size measurements: accuracy: better than ±2% on NIST traceable latex standards, precision/repeatability: better than ±2% on NIST traceable latex standards, ζ potential measurements: accuracy −0.12 μm cm V^{-1} s^{-1} for aqueous systems using NIST SRM1980 standard reference material.

TEM and EDX Spectroscopy

The morphology and crystal structure of the AuNPs were investigated by conventional TEM (JEOL 2100, JEOL ARM CF), STEM (JEOL ARM CF), electron diffraction (ED/TEM; JEOL 2100, JEOL ARM CF), and EDX spectroscopy/TEM (JED 2300). A drop of a colloidal suspension of AuNPs in deionized water was pipetted onto a carbon-coated TEM copper grid of 200 mesh and was dried in air at room temperature (Figure S6). Then, the dried sample of the AuNPs on a TEM grid was transferred to the TEM and analyzed with an 80 kV electron beam under high vacuum.

Measurement of Size and Circularity through TEM

The size and circularity measurements of the AuNPs were done with the help of TEM images in the following mentioned procedure. A minimum of 200 discrete AuNPs were measured from widely separated regions of the two samples to measure the size and circularity of the AuNPs from the TEM images according to Standard ISO 13322-1:2004. An ImageJ software tool was used for the data analysis algorithm.

UV/Vis Spectroscopy

The spectra of a colloidal solution of AuNPs were obtained by using quartz cells with a Varian Cary 100 Scan UV/Vis spectrophotometer. The initial parameters were: absorbance scan range: λ = 300–700 nm, number of reads = 5. Photometric accuracy for standard solution methods: ±0.01 Abs, wavelength accuracy at λ = 656.1 nm: λ ± 0.02 nm, wavelength accuracy at λ = 486.0 nm: λ ± 0.04 nm.

ICP-OES

Used for Au^{3+} quantification (i.e. concentration of Au in the AuNPs) in deionized water. Prior to analysis, samples were diluted tenfold with deionized Milli-Q water (purity 18 MΩ cm) and were acidified with aqua regia (5%, *v/v*). Single element standard solutions (Merck, Darmstadt, Germany) were used for calibration. Analysis was performed by using an ICP mass spectrometer (Agilent, 7500ce, equipped with a collision cell) under the operating conditions: RF power: −1.5 kW, sample depth: 8 mm, nebulizer: Meinhard, plasma gas flow: −15 L min^{-1}, nebulizer gas flow: −0.8 L min^{-1}, make up gas flow: −0.3 L min^{-1}, reaction gas flow: −4.0 mL min^{-1}.

Ion Chromatography

Before the measurements, the sample solution (pH of the sample solution was 5.4) was diluted tenfold with deionized water with a resistivity of 18 MΩ cm, obtained from a Milli-Q water purification system (Millipore, Bedford, MA, USA). For NO_2^- and NO_3^- determination, an ionic chromatography system Dionex, ICS 3000 was used under the following experimental conditions: eluent: 23 mM KOH, eluent source: EGC-KOH II cartridge, flow rate: 1 mL min^{-1}, temperature: 30 °C, detection: suppressed conductivity, suppressor: Dionex ERS 500, 4 mm; auto-suppression recycle mode, columns: Dionex IonPac AG 18 (4×50 mm) (precolumn) and Dionex IonPac AS 18 (4×250 mm), injection volume: 50 μL, pump flow rate precision: < 0.1%, pump flow rate accuracy: < 0.1%.

Statistics and Diagrams

Data are presented as a representative experiment or as a mean ± SD of at least three independent experiments. The differences between control experimental samples were analyzed by using the Kruskal–Wallis test with Bonferroni posttest, and values at $p < 0.05$ or less were considered to be statistically significant. Origin Pro 8 was used for plotting the graphs and figures.

Acknowledgements

This research was co-financed by the Ministry of Education, Science and Sport, Republic of Slovenia (Program MARTINA, OP20.00369 and Eureka project PRO-NANO E!11198). The authors acknowledge financial support from the Slovenian Research Agency (ARRS): Research Core Funding No. P2-0120, P2-0152, P2-0393, Z2-8161 and Infrastructure Program I0-0029.

Conflict of Interest

The authors declare no conflict of interest.

Keywords: characterization · gold · interactions · nanoparticles · ultrasonic spray pyrolysis

[1] K. Saha, S. S. Agasti, C. Kim, X. Li, V. M. Rotello, *Chem. Rev.* **2011**, *112*, 2739–2779.

[2] M. Notarianni, K. Vernon, A. Chou, M. Aljada, J. Liu, N. Motta, *Sol. Energy* **2013**, *106*, 23 – 37.
[3] D. Zhang, M. Wang, A. G. Brolo, J. Shen, X. Li, S. Huang, *J. Phys. D* **2013**, *46*, 024005.
[4] D. T. Thompson, *Nano Today* **2007**, *2*, 40 – 43.
[5] T. Zhang, H. Zhao, S. He, K. Liu, H. Liu, Y. Yin, C. Gao, *ACS Nano* **2014**, *8*, 7297 – 7304.
[6] M. Daniel, D. Astruc, *Chem. Rev.* **2004**, *104*, 293 – 346.
[7] R. Raliya, T. S. Chadha, K. Hadad, P. Biswas, *Curr. Pharm. Des.* **2016**, *22*, 2481 – 2490.
[8] R. Raliya, P. Biswas, *RSC Adv.* **2015**, *5*, 42081 – 42087.
[9] G. Chen, I. Roy, C. Yang, P. N. Prasad, *Chem. Rev.* **2016**, *116*, 2826 – 2885.
[10] M. P. Grzelczak, S. P. Danks, R. C. Klipp, D. Belic, A. Zaulet, C. K. Olsen, D. F Bradley, T. Tsukuda, C. Viñas, F. Teixidor, J. J. Abramson, M. Brust, *ACS Nano* **2017**, *11*, 12492 – 12499.
[11] O. Betzer, N. Perets, A. Angel, M. Motiei, T. Sadan, G. Yadid, D. Offen, R. Popovtzer, *ACS Nano* **2017**, *11*, 10883 – 10893.
[12] H. Kang, G. H. Lee, H. Jung, J. W. Lee, Y. Nam, *ACS Nano* **2018**, *12*, 1128 – 1138.
[13] S. Palmal, A. R. Maity, B. K. Singh, S. Basu, N. R. Jana, *Chem. Eur. J.* **2014**, *20*, 6184 – 6191.
[14] R. Raliya, D. Saha, T. S. Chadha, B. Raman, P. Biswas, *Sci. Rep.* **2017**, *7*, 44718.
[15] X. Huang, I. H. El-sayed, M. A. El-sayed, *Nanomedicine* **2007**, *2*, 681 – 693.
[16] Y. Su, Y. Ke, S. Cai, Q. Yao, *Light: Sci. Appl.* **2012**, *1*, 2 – 6.
[17] J. Song. L. Wang, A. Zibart, C. Koch, *Metals* **2012**, *2*, 450 – 477.
[18] H. N. Mcquaid, M. F. Muir, L. E. Taggart, S. T. McMahon, J. A. Coulter, W. B. Hyland, S. Jain, K. T. Butterworth, G. Schettino, K. M. Prise, D. G. Hirst, S. W. Botchway, F. J. Currell, *Sci. Rep.* **2016**, *6*, 19442.
[19] S. K. Vishwakarma, P. Sharmila, A. Bardia, *Sci. Rep.* **2017**, *7*, 8539.
[20] M. R. Langille, M. L. Personick, J. Zhang, C. A. Mirkin, *J. Am. Chem. Soc.* **2011**, *133*, 10414 – 10417.
[21] Y. C. Wang, S. Gunasekaran, *J. Nanopart. Res.* **2012**, *14*, 1200.
[22] B. Liu, M. Louis, L. Jin, G. Li, J. He, *Chem. Eur. J.* **2018**, *24*, 9651 – 9657.
[23] N. G. Bastus, J. Comenge, V. Puntes, *Langmuir* **2011**, *27*, 11098 – 11105.
[24] G. Schmid, B. Corain, *Eur. J. Inorg. Chem.* **2003**, 3081 – 3098.
[25] B. Jin, H. Bang, K. S. Suslick, *Adv. Mater.* **2010**, *22*, 1039 – 1059.
[26] S. H. Choi, J. H. Lee, Y. C. Kang, *ACS Nano* **2015**, *9*, 10173 – 10185.
[27] B. Weidenhof, M. Reiser, K. Stowe, W. F. Maier, M. Kim, J. Azurdia, *J. Am. Chem. Soc.* **2009**, *131*, 9207 – 9219.
[28] S. K. Kim, H. Kim, H. Chang, B. G. Cho, J. Huang, H. Yoo, H. Kim, H. D. Jang, *Sci. Rep.* **2016**, *6*, 33688.
[29] M. Garza, T. Hernández, R. Colás, I. Gómez, *Mater. Sci. Eng. B* **2010**, *174*, 9 – 12.
[30] R. J. Lang, *J. Acoust. Soc. Am.* **1962**, *34*, 6 – 8.
[31] J. Bogovic, *Synthesis of the Oxide and Metal/Oxide Nanoparticles by the Ultrasonic Spray Pyrolysis*, PhD Dissertation, Faculty of the Georesources & Materials Engineering, RWTH Aachen University, Aachen, **2015**.
[32] P. Majerić, D. Jenko, B. Friedrich, R. Rudolf, *Adv. Powder Techn.* **2017**, *28*, 876 – 883.
[33] P. Majerič, D. Jenko, B. Budič, S. Tomić, M. Čolić, B. Friedrich, R. Rudolf, *Nanosci. Nanotechnol. Lett.* **2015**, *7*, 920 – 929.
[34] R. Rudolf, P. Majerič, S. Tomić, M. Shariq, U. Ferčec, B. Budič, B. Friedrich, D. Vučević, M. Čolić, *J. Nanomater.* **2017**, 9365012.
[35] R. Rudolf, B. Friedrich, S. Stopić, I. Anžel, S. Tomić, M. Čolić, *J. Biomater. Appl.* **2012**, *26*, 595 – 612.
[36] H. Wu, C. Kuo, M. H. Huang, *Langmuir* **2010**, *26*, 12307 – 12313.
[37] M. Haruta, S. Tsubota, T. Kobayashi, H. Kageyama, M. J. Genet, B. Delmon, *J. Catal.* **1993**, *144*, 175 – 192.
[38] S. Ivanova, V. Pitchon, Y. Zimmermann, C. Petit, *Appl. Catal. A* **2006**, *298*, 57 – 64.
[39] M. Bowker, A. Nuhu, J. Soares, *Catal. Today* **2007**, *122*, 245 – 247.
[40] J. D. Lessard, I. Valsamakis, M. F. Stephanopoulos, *Chem. Commun.* **2012**, *48*, 4857 – 4859.
[41] A. Hugon, El-N. Kolli, C. Louis, *J. Catal.* **2010**, *274*, 239 – 250.
[42] H. D. Glicksman, T. T. Kodas, D. Majumdar, *Method for Making Gold Powders by Aerosol Decomposition*, US 5616165 A, **1997**.
[43] X. Lu, H. Y. Tuan, B. A. Korgel, Y. Xia, *Chem. Eur. J.* **2008**, *14*, 1584 – 1591.
[44] M. Behera, S. Ram, *Appl. Nanosci.* **2013**, *3*, 83 – 87.
[45] W. Luo, P. Gobbo, C. D. McNitt, D. A. Sutton, V. V. Popik, M. S. Workentin, *Chem. Eur. J.* **2017**, *23*, 1052.
[46] Alfa Aesar: Gold Acetate. https://www.alfa.com/en/catalog/039742/ (accessed March 30, **2018**).
[47] American Elements: Gold Nitrate. https://www.americanelements.com/gold-nitrate-13464-77-2 (accessed March 30, **2018**).
[48] American Elements: Gold Oxide. https://www.americanelements.com/gold-oxide-1303-58-8 (accessed March 30, **2018**).
[49] H. Sakurai, K. Koga, Y. Iizuka, M. Kiuchi, *Applied Catal A* **2013**, *462*, 236 – 246.
[50] M. Shariq, P. Majerič, B. Friedrich, B. Budic, A. R. Dixit, R. Rudolf, *J. Cluster Sci.* **2017**, *28*, 1647 – 1665.
[51] L. Zhu, C. Zhang, C. Guo, X. Wang, P. Sun, D. Zhou, W. Chen, G. Xue, *J. Phys. Chem. C* **2013**, *117*, 11399 – 11404.
[52] D.-S. Wang, T. Xie, Q. Peng, S.-Y. Zhang, J. Chen, Y.-D. Li, *Chem. Eur. J.* **2008**, *14*, 2507 – 2513.
[53] S. Yuvaraj, L. F. Yuan, C. T. Huei, Y. C. Tih, *J. Phys. Chem. B* **2003**, *107*, 1044 – 1047.
[54] K. H. Stern, *J. Phys. Chem. Ref. Data Monogr.* **1972**, 747 – 772.
[55] G. L. Messing, S. Zhang, G. V. Jayanthi, *J. Am. Ceram. Soc.* **1993**, *76*, 2707 – 2726.
[56] T. T. Kodas, M. Hampden-Smith, *Aerosol Processing of Materials*, 1st ed., Wiley-VCH, New York, **1998**.
[57] P. Majerić, *Synthesis of Gold Nanoparticles with a Modified Ultrasonic Spray Pyrolysis*, PhD Dissertation, Faculty of Mechanical Engineering, University of Maribor, Slovenia, **2016**.
[58] J. H. Bang, K. S. Suslick, *Adv. Mater.* **2010**, *22*, 1039 – 1059.
[59] I. W. Lenggoro, T. Hata, F. Iskandar, M. M. Lunden, K. Okuyama, *J. Mater. Res.* **2000**, *15*, 733.
[60] S. Chaturvedi, P. N. Dave, *J. Energ. Mater.* **2012**, *31*, 1 – 26.
[61] D. Bennett, *J. Appl. Chem.* **1972**, *22*, 973 – 982.
[62] R. D. Smith, *Trans. Faraday Soc.* **1957**, *53*, 1341 – 1345.
[63] P. Lin, S. Lin, P. C. Wang, R. Sridhar, *Biotechnol. Adv.* **2014**, *32*, 711 – 726.
[64] J. Lee, J. Yang, S. G. Kwon, T. Hyeon, *Nat. Rev. Mater.* **2016**, 16034.
[65] M. H. Fonticelli, E. Zelaya, J. C. Azcarate, *J. Phys. Chem. C* **2017**, *121*, 26108 – 26116.
[66] C. Gutiérrez-wing, J. A. Olmos-asar, R. Esparza, M. M. Mariscal, M. J. Yacamán, *Electrochim. Acta* **2013**, *101*, 301 – 307.

Received: May 31, 2018
Revised manuscript received: June 20, 2018

